Relative importance of polaron activation and disorder on charge transport in high-mobility conjugated polymer field-effect transistors

Jui-Fen Chang and Henning Sirringhaus*

Cavendish Laboratory, University of Cambridge, Madingley Road, Cambridge CB3 0HE, United Kingdom

Mark Giles, Martin Heeney, and Iain McCulloch

Merck Chemicals, University Parkway, Chilworth Science Park, Chilworth, Southampton SO16 7QD, United Kingdom

The charge transport properties of conjugated polymer semiconductors are governed by strong electron phonon coupling, leading to polaron formation as well as the presence of structural and electronic disorder. However, the relative contribution which polaronic relaxation and disorder broadening make to the temperature activation of the mobility of these materials is not well understood. Here we present a combined study of the temperature and concentration dependences of the field-effect mobility and the optically induced electron-transfer transitions of a series of poly(3-hexylthiohene) field-effect transistors of different molecular weight. We apply a vibronic coupling model to extract the reorganization energy and the strength of electronic coupling from the optical spectra. We observe a transition from a localized to a delocalized transport regime as a function of molecular weight and crystalline quality. Polaron activation is comparable to disorder-induced activation in the low-mobility regime $[\sim 10^{-3} \text{ cm}^2/(\text{V s})]$ and needs to be taken into account when interpreting the field-effect mobility, while disorder becomes the dominant mechanism to limit charge transport in the high-mobility regime with mobilities $> 10^{-2} - 10^{-1} \text{ cm}^2/(\text{V s})$.

I. INTRODUCTION

Over the past decades, the charge transport mechanism in disordered organic solids has been extensively analyzed on the basis of two different theoretical frameworks. One assumes transport to be dominated by energetic and positional disorder, and the other one considers polaronic relaxation effects due to strong electron-phonon coupling to be important. The disorder theories[1–4] assume a sufficiently weak electron-phonon coupling and attribute the activation energy of the charge mobility mainly to the broadening of the density of states as a result of static energetic disorder of the hopping sites. Alternatively, the polaron theories[5–11] consider a strong electron-phonon coupling with the disorder being of secondary importance and relate the activation energy of the charge mobility to the polaron binding energy. The disorder and polaron-based theories have been applied to explain the electric-field and temperature dependences of the mobility observed in molecularly doped polymer systems for xerographic applications.[12–17] Neither of these theories can fully describe the field and temperature dependences of the mobility over the range observed experimentally. In the case of disorder-based theories it has been shown that it is important to consider spatial correlations of disorder[18] and the concentration dependence of the mobility[19] in order to explain the observed field dependence of the mobility. Polaron theories predict physical parameters such as polaron binding energies and transfer integrals to be unacceptably large.[13] From the significant body of work on xerographic systems there is a consensus that molecularly doped polymers are dominated by disorder and that polaron effects do not manifest themselves strongly in the observable electrical transport properties.[20,21]

A more complete model of transport properties in organic systems, however, should include both disorder and polaron effects. Bässler *et al.* suggested that at zero electric field the total activation energy of mobility can be approximated by a sum of the disorder and polaron contributions.[22] Also, Kenkre and Dunlap[23,24] proposed an analytical model in which the polaronic transport is a minor effect under the influence of energetic disorder, although this model also yields unacceptably large values of polaron binding energies and transfer integrals. More recently, Parris *et al.*[25] solved the problem related to the magnitude of physical parameters in small polaron transport by assuming the presence of correlated energetic disorder. Fishchuk *et al.*[26] further derived an analytical model to distinguish the polaron and polaron-free transport in a disordered organic semiconductor.

Most of the previous work has focused on molecularly doped polymers, and the disorder and polaron effects were investigated experimentally by measuring the temperature- and electric-field dependences of the mobility in a diode configuration using the time-of-flight technique. Much less is known about the relative importance of disorder and polaronic relaxation effects in conjugated organic molecules and polymers. These have recently become of significant scientific and technological interest for applications such as active layers in organic field-effect transistors (FETs).[27] There can be little doubt that a significant degree of disorder is present in a solution-processed polymer semiconductor film. On the other hand, there has also been direct and unambiguous evidence from optical spectroscopy measurements of the field-induced charges that the charge carriers carrying the current in the accumulation layer of the FET are localized polarons.[28] How polaron and disorder effects manifest themselves in the electrical characteristics of the FET is not well understood. We emphasize that the transport physics of self-organized conjugated polymer semiconductors with mobilities approaching 0.1 cm^2/(V s) could be different from that

of amorphous molecularly doped polymers with mobilities less than 10^{-2}–10^{-3} cm^2/(V s), because the former are often semicrystalline polymers with a high degree of local self-organization. Furthermore, the understanding of polaron effects is generally an important issue when aiming to improve the performance of polymer devices by searching for polymer materials with better intrinsic transport properties.[29] In the present work we aim to investigate if and how polaronic relaxation effects manifest themselves in the electrical characteristics of polymer field-effect transistors based on poly(3-hexylthiophene) (P3HT), one of the most studied and highest performing semiconducting polymers. We investigate the temperature and gate voltage dependences of the FET mobility and aim to understand these in terms of the disorder broadened density of states and the polaron activation energy of the polymer. (The polaron activation energy is defined as being half of the polaron binding energy in nonadiabatic, small polaron transport while it depends on both the binding energy and electronic coupling integral in the adiabatic transport regime; see Sec. III.) Following our recent study,[30] a series of polymers with different molecular weight (MW) are used to vary the mobility and the degree of interchain polaron delocalization.

Simple fitting of the electrical FET characteristics to a transport model incorporating both polaron as well as disorder effects is unlikely to yield unambiguous insight, since both factors manifest themselves in qualitatively similar ways; i.e., they both tend to lead to a thermally activated mobility. Therefore, a technique is needed that is able to independently investigate and quantify the polaron activation energy. In the early studies of mixed-valence systems,[31,32] it was found that molecular systems containing ions in different oxidation states often have a unique class of electronic absorption spectra appearing in the visible or near-infrared region, which cannot be attributed to the absorption of either constituent ion. This low-energy absorption band, termed a charge-transfer (CT) band[33] or a mixed-valence (intervalence) band,[34] has a signature associated with the characteristic parameters of the electron-transfer (ET) process between different oxidation states involving molecular vibrations and depends on the extent of charge delocalization. Marcus and Sutin[35–37] developed a theory for weakly coupled electronic systems where the barrier for ET can be estimated from two parameters: the vertical reorganization energy λ and the electronic coupling integral J. Robin and Day[38] further classified the ET between mixed-valence complex into three categories: completely localized (class I, where $J=0$), weakly coupled, localized (class II, where $2J \ll \lambda$), and strongly coupled, delocalized (class III, where $2J > \lambda$) regimes. Hush[39,40] then extended the Marcus theory for estimating both λ and J from intervalence CT absorption spectra in weakly coupled systems. Recently, the mixed-valence behavior has also been observed in polymer systems with strong interchain interaction such as P3HT, as evidenced by the appearance of a midinfrared CT transition induced by strong interchain interactions.[41–44] The quantum-chemical calculations have further demonstrated that the CT transition observed in P3HT films involves electron transfer between neighboring polymer chains; i.e., the transition is

predicted to be polarized along the interchain packing direction and the intensity of the absorption feature is related to the amount of interchain delocalization of the polaron wave function.[45] Here we use charge modulation spectroscopy[41,42] to determine experimentally the CT transition in P3HT polymers of different MW. We use a vibronic coupling model developed by Piepho[46–48] to fit the spectra and extract the important transport parameters related to λ and J. This vibronic model can be applied for the full range of mixed-valence systems from localized (class II) to delocalized (class III) regimes.[49] In this way we can independently determine the degree of polaron localization and polaron activation energy, and use this as an input parameter to interpret the electrical transport measurements. This allows us to investigate to which degree polaronic relaxation effects manifest themselves in the electrical characteristics of P3HT FETs of different MW.

The paper is organized as follows: In Sec. II we present the low-temperature FET measurements for polymers of different molecular weight and extract the activation energy of the field-effect mobility. In Sec. III we describe the corresponding Fourier-transform-infrared charge modulation spectroscopy (FTIR CMS; see Refs. 41 and 42) and measurements of the CT transitions of field-induced charge in the midinfrared spectral range and the parameter extraction using a vibronic coupling model. A clear transition from localized to delocalized polaronic transport is observed between low- and high-MW polymers. In Sec. IV we incorporate the estimated polaron activation energy into the mobility-edge model to extract the distribution of localized states and mobility prefactor from temperature-dependent transport data. The results are discussed in Sec. V.

II. TEMPERATURE-ACTIVATED CHARACTERIZATION

The low-temperature measurements were performed on bottom-gate, bottom-contact FETs. A heavily n-doped silicon substrate acts as a common gate contact and a 200-nm thermal oxide as gate dielectric. A series of FET devices with mobilities ranging from 10^{-3} to 10^{-1} cm^2/(V s) at room temperature were prepared by choice of molecular weights and solvents. Regioregular P3HT of different MW was synthesized by the transition-metal-mediated cross coupling of a 2,5-dibromo 3-hexylthiophene monomer under a range of catalytic and coreagent conditions.[50] All the polymers have a consistently high regioregularity and low level of ionic impurities (the details can be referred to in Ref. 30). Since our previous work has shown that mobilities increase sharply from 15 kD to 40 kD and saturate at the order of 0.1 cm^2/(V s) for even higher MW in highly crystalline films, we choose three different MW polymers (15 kD, 37 kD, and 270 kD) and 1,2,4-trichlorobenzene (TCB) as the solvent to obtain highly crystalline devices with mobilities of 3×10^{-3}, 5×10^{-2}, and 0.1 cm^2/(V s), respectively. To avoid the complication of the temperature dependence by contact resistance effects that are important in short-channel devices (<5 μm),[51] we used a long channel length $L=20$ μm, and the channel width (W) is fixed at 1 cm. Before cooling the devices were annealed at 70 °C for 2–3 h in a vacuum
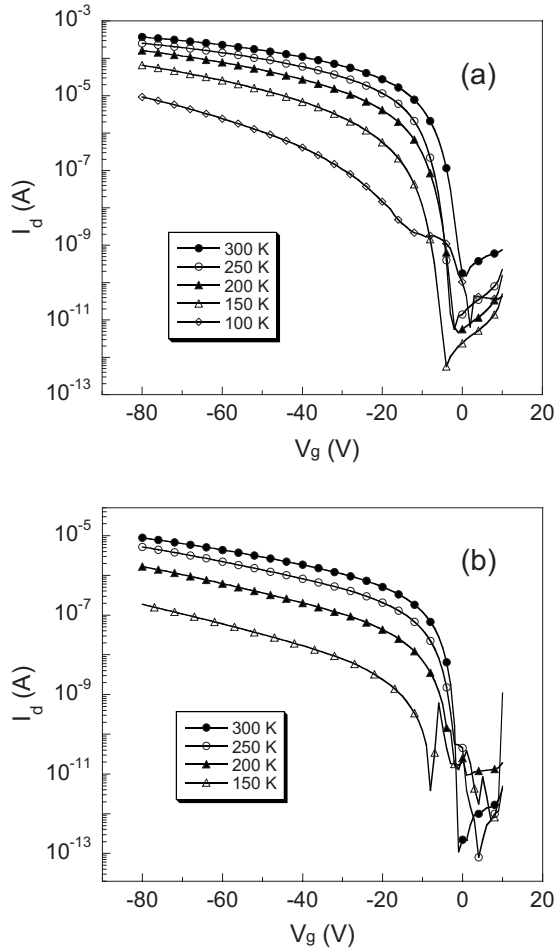
FIG. 1. Transfer characteristics ($V_{ds}=-5$ V) of TCB spin-cast transistors with MW of (a) 270 kD and (b) 15 kD at different temperatures on a semilog$_{10}$ scale.

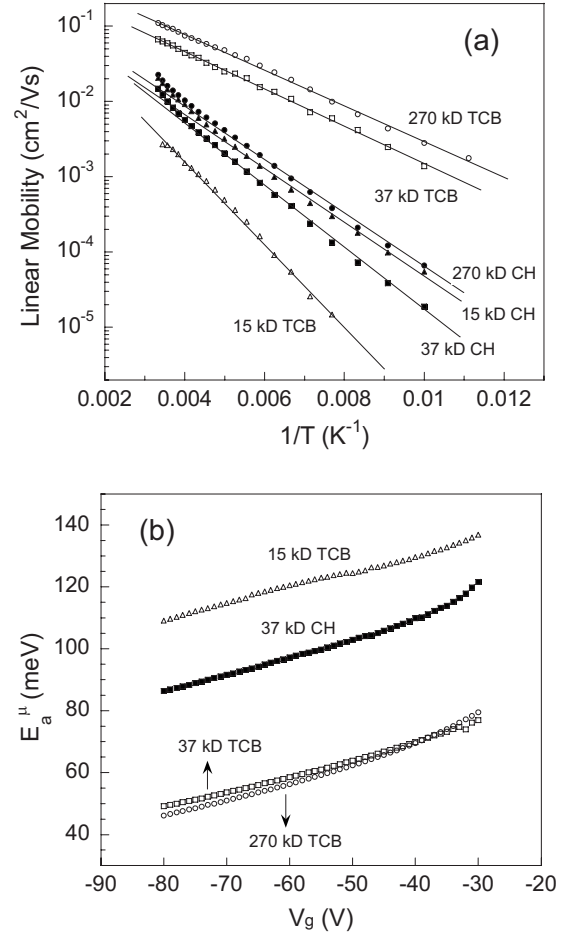FIG. 2. (a) Field-effect mobility vs inverse temperature extracted from the linear transfer characteristics ($V_{ds}=-5$ V) of P3HT FETs at $V_g=-80$ V for 270-kD, 37-kD, and 15-kD MW polymers. Open and solid symbols denote the TCB and chloroform spin-cast devices, respectively. (b) Activation energy of the field-effect mobility vs V_g for devices with different MW and solvents.

chamber to remove residual solvents and volatile, unintentional dopants induced by moisture and oxygen exposure. The electrical characteristics were measured in the pulsed mode, where a short pulse ($\sim$ms) was applied to the gate electrode to minimize any effect of unintended bias stressing that might modify the extracted temperature and gate-voltage dependences of the mobility.[52] All measurements were performed under high vacuum ($P \sim 10^{-7}$ torr) and in darkness.

Figure 1 shows the temperature dependence of the linear transfer characteristics of the high-MW [270 kD (a)] and low-MW [15 kD (b)] TCB spin-cast devices. The onset voltage of both devices is close to 0 V at room temperature, and no significant shift is observed as temperature decreases. This is consistent with the observation by Meijer *et al.*[53] The linear mobility was calculated by the description of the "effective mobility,"[52,54] where all the mobile and immobile carriers are taken into account by applying the approximation that the onset voltage V_{on} is close to zero and independent of temperature:

$$\mu_{eff}(V_g,T) = \frac{I_d}{C_i V_{ds}(V_g - V_{on})}\frac{L}{W} \approx \frac{I_d}{C_i V_{ds}V_g}\frac{L}{W}, \qquad (1)$$

where C_i is the gate dielectric capacitance. This description of mobility rules out the temperature dependence of threshold voltage, somewhat different from a conventional equation where the mobility is determined only for the mobile carriers:[55]

$$\mu_{TFT}(V_g,T) = \frac{L}{WC_i V_{ds}}\left(\frac{\partial I_d}{\partial V_g}\right)_{V_{ds}\to 0}. \qquad (2)$$

In the latter expression the gate-voltage-dependent mobility is extracted from the transconductance ($\partial I_d/\partial V_g$) of the transfer curves. At high temperature $\mu_{TFT} \sim \mu_{eff}$ at sufficiently high gate voltage if the device exhibits linear dependence of the current on gate voltage, while at low temperature $\mu_{TFT} > \mu_{eff}$ over the whole range of gate voltage as the transfer characteristics become superlinear.

Figure 2(a) shows the temperature dependence of the linear mobility calculated from Eq. (1) for different MW devices. Control devices spin-cast from chloroform [$\mu \sim 0.01$ cm^2/(V s) at room temperature, independent of MW] were also provided for each MW polymer. As previ-

ously demonstrated, sufficiently high-MW polymers (270 kD and 37 kD) polymers spin-cast from TCB have significantly higher mobilities than those spin-cast from chloroform due to the formation of preferentially in-plane oriented π-π stacking and a higher degree of crystallinity.[56] On the contrary, low-MW polymers (15 kD) spin-cast from TCB have lower mobilities than spin-cast from chloroform probably due to the presence of more tie molecules linking crystallites in the chloroform films.[30] Moreover, we find that for a fixed MW polymer the temperature dependence is slightly different for TCB and chloroform spin-cast devices. All the highly crystalline TCB devices exhibit simple Arrhenius activation [$\mu \propto \exp(-E_a^\mu/kT)$, where E_a^μ is an apparent activation energy of the field-effect mobility] between 100 K and 300 K. However, the temperature dependence of the chloroform devices generally appears to be nonmonotonic. Below 250 K the mobilities approximately follow the Arrhenius rule as the TCB devices, whereas above 250 K the mobilities increase with temperature with a steeper slope than in the lower-temperature regime. This behavior is reproducible. Street *et al.* explained that the change of slope in the temperature dependence may be related to a nonzero band-tail mobility in the mobility-edge model.[54] Note that the more disordered films deposited from chloroform are expected to have a broader density of states and less well-defined mobility edge between conduction band and trap states. In general, we observed that the mobilities of P3HT decrease above 350–370 K probably due to the relaxation of polymer morphology.[57]

Figure 2(b) shows the activation energy of the field-effect mobility, E_a^μ, as a function of gate voltage extracted between 250 K and 100 K for different MW polymers. The chloroform device is only shown for the case of 37 kD polymer because of the similarity between different MW polymers. At sufficiently high gate voltages, 270-kD TCB and 37-kD TCB devices have very similar E_a^μ around 50–60 meV, much lower than the 37-kD chloroform device (90–100 meV) and the 15-kD TCB device (110–120 meV).

According to the theory by Bässler and co-workers,[22,58] the activation energy of mobility can be approximated in lowest order by a sum of the disorder and polaronic contributions. Since the degree of structural disorder in crystalline films is nearly independent of MW or even slightly decreases in high-MW polymers,[30] the strong MW dependence of E_a^μ suggests that polaronic contributions to activated charge transport could be more essential in lower-MW polymers. To achieve a quantitative understanding of the polaronic contribution to the activated transport in different MW polymers, we now proceed to extract the polaron activation energy by analyzing the spectra of CT transitions measured by CMS with a dynamic vibronic model, as described below.

III. CHARGE-TRANSFER TRANSITION

Figure 3 shows the FTIR CMS spectra measured using a FTIR spectrometer on bottom-gate, top-contact FET devices. The device structure and observed mobilities were very similar as for the bottom-contact devices [Fig. 2(a)] used for the low-temperature measurements, the only difference being
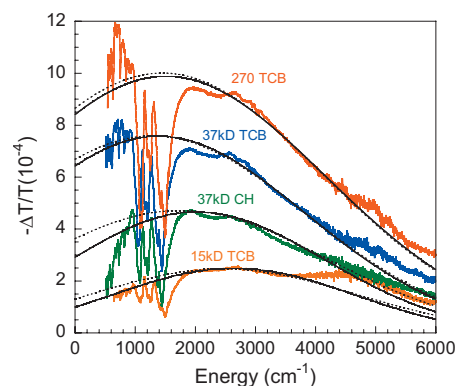

FIG. 3. (Color) Experimental FTIR CMS spectra (colored lines) and calculated absorption profiles from Piepho's model (solid lines) and the PKS model (dotted lines).

that a top-contact gold source-drain interdigitated electrode was evaporated onto the P3HT film for the CMS measurements. The CMS spectra were extracted from the difference of infrared transmission spectra with the device being dc-biased alternately in the accumulation ($V_g = -30$ V) and depletion ($V_g = 10$ V) regimes, taking typically ca. 20 000 averages. From these we can construct the charge-induced absorption spectrum in a spectral range of 500–6000 cm^{-1}. The spectra exhibit a broad polaronic electronic transition peaking at energies of 500–3000 cm^{-1}, on which a series of sharp dips are superimposed. The latter have been interpreted previously as (anti)resonances between the infrared-active vibrational modes of the polymer and the broad polaronic excitation.[59,60] They are present in all samples studied, but are not further analyzed here. The focus of our analysis here is on understanding the intensity and peak position of the broad CT electronic transition which appears to be closely correlated with the field-effect mobility. The highest-mobility 270 kD TCB device exhibits the most intense CT transition centered around or below 700 cm^{-1}. The lower-energy cutoff of our experiments at 500 cm^{-1} is limited by the low transmission of the silicon substrate and the reduced sensitivity of the detector at lower energies, and we are unable to determine accurately where the transition peaks in these high-mobility samples. In the 37-kD TCB device with a slightly lower mobility, the transition is less intense but appears to peak at similar energies as in the 270-kD TCB device. By contrast, 37-kD chloroform and 15-kD TCB devices with significantly lower mobilities have a significantly reduced intensity and higher energy of the CT transition.

The theoretical framework used to interpret the experimental CT spectra of P3HT transistors is based on a vibronic coupling model developed by Piepho.[47,48] This model (hereafter referred to as Piepho's model and which is physically equivalent to the Holstein-Peierls polaron models[61,62]) was advanced from the Piepho-Krausz-Schatz (PKS) model[46] by including the multicenter vibrations in the vibronic coupling of bridged mixed-valence compounds. The absorption profile of the CT bands can be obtained by calculating the complete manifold of the transition intensities from the populated vibronic levels to all higher vibronic levels. Piepho's model has recently been applied to investigate the CT transitions in

pure organic mixed-valence systems with significant electronic coupling,[49,63] and also demonstrated to provide a better fit to experimental spectra than the original PKS model. Following a similar procedure as in Ref. [49], here we consider a simplified two-mode vibronic model that contains a symmetric vibration and an antisymmetric vibration, where only two electronic states ψ_+ (symmetric) and ψ_- (antisymmetric) with energy ε_+ and ε_- are involved in the CT transitions. The vibronic Hamiltonian of the system in the electronic basis of ψ_+ and ψ_- is described by

$$H = \begin{pmatrix} T_+ + T_- + \dfrac{1}{2}(k_+ Q_+^2 + k_- Q_-^2) & l_- Q_- \\[2mm] l_- Q_- & T_+ + T_- + \dfrac{1}{2}(k_+ Q_+^2 + k_- Q_-^2) + \Delta + l_+ Q_+ \end{pmatrix}. \tag{3}$$

Here Q_+ and Q_- are the symmetric and antisymmetric molecular coordinates, T_+ and T_- are the kinetic energy of the nuclei, and k_+ and k_- are the force constants (assumed the same in both electronic states). $\Delta = \varepsilon_+ - \varepsilon_-$ is the energy difference between the electronic states $\psi_\pm$, related to the electronic coupling integral J by $J = \Delta/2$. l_+ is the diagonal vibronic constant related to the relaxation energy L by $L = l_+^2/2k_+$, and l_- is the off-diagonal vibronic constant related to the Marcus reorganization energy λ by $\lambda = 2l_-^2/k_-$.

Typical adiabatic potential surfaces associated with the mixed valence transitions can be calculated by diagonalizing the vibronic matrix without considering the nuclear kinetic energy and diagonal vibronic coupling:

$$E_1(Q_-) = \frac{1}{2}\left(k_- Q_-^2 + \Delta + \sqrt{\Delta^2 + 4l_-^2 Q_-^2}\right),$$

$$E_2(Q_-) = \frac{1}{2}\left(k_- Q_-^2 + \Delta - \sqrt{\Delta^2 + 4l_-^2 Q_-^2}\right). \tag{4}$$

In the weak electronic coupling regime where $\lambda = 2l_-^2/k_- > \Delta$, the lower adiabatic surface E_2 possesses two equivalent minima at $Q_-^{\min} = \pm\sqrt{(\lambda^2 - \Delta^2)/2\lambda k_-}$, each of which corresponds to the situation when the system is localized on one of the valence structures. According to Marcus' theory,[36,64] electrons can transfer through the same nuclear configuration from a minimum in the lower adiabatic surface to the Frank-Condon state of the upper adiabatic surface by optical excitation. This process requires a reorganization energy of $E_1(Q_-^{\min}) - E_2(Q_-^{\min}) = \lambda$, corresponding to the peak energy of the CT optical transition as predicted by Hush.[40,65] Electron transfer may also follow another energetically less expensive pathway involving thermal activation in the lower adiabatic surface. This process requires an activation energy

$$E_a = E_2(0) - E_2(Q_-^{\min}) = \frac{(\lambda - \Delta)^2}{4\lambda}. \tag{5}$$

In the limit of nonadiabatic electron transition (class I), $\Delta = 0$ and the activation energy is $E_a = \lambda/4$. For a very weak electronic coupling system (class II), $\Delta \ll \lambda$ and the activation energy can be approximated by $E_a \approx \lambda/4 - \Delta/2 = E_b/2$

$-J$, where $E_b = \lambda/2$ is the polaron binding energy. However, in the strongly coupled systems where $\Delta > \lambda$ (class III), the lower adiabatic surface E_2 possesses only one minimum at $Q_- = 0$. This indicates that the charge may move freely between neighboring molecules without reorganization of the involved molecular configurations. In this delocalized system the Hush theory breaks down and the peak energy of the CT transition becomes a direct measure of the electronic coupling Δ but weakly relates to λ.[66]

The eigenvalues and eigenfunctions of the vibronic matrix were solved by the numerical procedure as described in Ref. [47]. The total number of vibrational quanta used in the calculation was 20. Since previous experiments[41,45] have shown that the strength of the CT transition is a measure of polaron delocalization over neighboring chains, we presume that the electron transfer in P3HT is primarily mediated by *interchain* vibrational modes. The energy $\hbar\omega_-$ of the antisymmetric vibrational mode (the effective mode coupling to the ET process) was assumed to be 100 cm^{-1}, taken from an average value of the low-frequency modes that couple to the intermolecular transfer integral in organic crystals.[67] On the other hand, the energy $\hbar\omega_+$ of the symmetric vibrational mode was set as 1450 cm^{-1}, taken to be the C=C stretch deformation that is most sensitive to the excitation energy.[68] Each vibronic line is assumed to be of Gaussian line shape $f_l(E)$ with the same linewidth Γ:

$$f_l(E) = \frac{\exp[-(E - E_l)^2/\Gamma^2]}{\Gamma\sqrt{\pi}}, \tag{6}$$

where E_l is the calculated energy for each line. The CT spectra were then simulated by summing all the transition intensities from lower to higher vibronic lines with λ, L, and Δ as free parameters. A sufficiently large Γ is used to produce smooth bands.

The best fitting results of Piepho's model are shown in Fig. [3] (solid lines), along with those obtained by the PKS model with only the nondiagonal vibronic interaction[46] (dotted lines). The fitting parameters are given in Table [I]. It shows that Piepho's model allows one to obtain slightly better fits for all the devices compared with the PKS model. The PKS model also fits reasonably well for the high-mobility

TABLE I. Parameters extracted from fitting the experimental CT spectra in Fig. 3 to (a) Piepho's model and (b) the PKS model. The energy of symmetric and antisymmetric vibrational modes are assumed to be 1450 cm^{-1} and 100 cm^{-1}, respectively. The polaron activation energy E_a is estimated from Eq. (5). The fitting errors of λ are about ± 200 cm^{-1} for 15-kD TCB and 37-kD chloroform devices, but cannot be accurately assessed for the high-mobility devices. The errors of Δ and L are about ± 50 cm^{-1}. Within the range of fitting errors the variation of the estimated E_a is less than 10 meV and 1 meV for 15-kD TCB and 37-kD chloroform devices, respectively.

	μ_{FET} [cm^2/(V s)]	$\lambda^{(a)}$ [cm^{-1}]	$L^{(a)}$ [cm^{-1}]	$\Delta^{(a)}$ [cm^{-1}]	$\lambda^{(b)}$ [cm^{-1}]	$\Delta^{(b)}$ [cm^{-1}]	$E_a^{(a)}$ [meV]	$E_a^{(b)}$ [meV]
270 kD TCB	0.1	300	100	1380	300	1400	–	–
37 kD TCB	0.05	600	150	1080	700	1120	–	–
37 kD CH	0.01	1300	350	870	2000	1010	4.4	15.2
15 kD TCB	0.003	2100	270	670	3100	820	30.2	52.0

devices, but the low-energy side of the CT band in low-mobility devices cannot be well reproduced. However, the difference between the two models is rather small, and on the basis of our results we cannot draw strong conclusions regarding the need to include multicenter vibration modes in the model. The high-MW TCB devices exhibit the largest value of Δ and the smallest value of λ. This is consistent with previous studies which have demonstrated strong interchain interactions in high-mobility P3HT.[41,42,45] In devices with lower mobilities Δ has to be reduced to account for the decreased intensity and λ has to be increased to account for the blueshift of the CT band. Our calculation also reveals that devices with lower mobilities appear to have higher relaxation energies L, as increasing diagonal vibronic constants may enhance the transitions to higher vibronic levels, resulting in slight band asymmetry—a decrease in the low-energy side of CT and an increase in the high-energy side of CT. In high-mobility devices similar values of λ and Δ are obtained in the two models because L is much lower than Δ and has little effect on λ and Δ. However, in low-mobility devices the increase in L/Δ leads to Δ and λ remarkably smaller than those predicted by the PKS model. As a result, the polaron activation energy derived from Piepho's model is significantly lower compared to the PKS model. Although the effect of L on electron transfer is unknown, the parameter values extracted from these two models are expected to yield a reasonable range for estimation of polaron activation energy. We prefer to adopt the parameter values extracted from Piepho's model because not only a better fit is obtained but also the parameter values used in the remainder of this work provide very consistent results.

Importantly, the fitting results in both models reveal a crossover between localized and delocalized transport as mobility increases from 10^{-3} to 10^{-1} cm^2/(V s). For clarity in Fig. 4 we show the adiabatic potential surfaces solved by Eq. (4) for 15-kD and 270-kD TCB devices, where the values of λ and Δ are taken from those extracted by Piepho's model. The 15-kD device is in the localized regime where $\Delta < \lambda$ (class II), and the peak energy of CT transition close to the value of λ agrees with the Hush theory. In this case we estimate the polaron activation energy E_a from Eq. (5) to be on the order of 247 cm^{-1} ($\sim$30 meV). The 37-kD chloroform device appears to be located in the intermediate regime

between classes II and III as λ is slightly larger than Δ. E_a is estimated to be around 5 meV, significantly lower than that of the 15-kD TCB device. The high-mobility devices (270-kD TCB and 37-kD TCB) are apparently in the delocalized regime where $\Delta > \lambda$ (class III). The peak energy of the CT transition is close to the value of Δ but relatively insensitive to λ. In these two systems the polarons are delocalized over a number of interacting polymer chains and the polaron activation energy is approximately zero.

We can compare the values of E_a due to the polaronic relaxation estimated from the CT transition with the experimentally observed activation energy of the field-effect mobility, E_a^μ. E_a contributes roughly 25% of E_a^μ in low-MW, low-mobility devices, but less than 5% of E_a^μ in the chloroform device, and in the highly crystalline, sufficiently high-MW devices with even higher mobilities polaronic relaxation makes no contribution to the activation energy of the field-effect mobility. This strongly suggests that polaron hopping needs to be considered in order to describe the low-mobility regime [10^{-3} cm^2/(V s)], whereas disorder becomes the only transport-limiting mechanism in the high-mobility regime [10^{-2}–10^{-1} cm^2/(V s)].
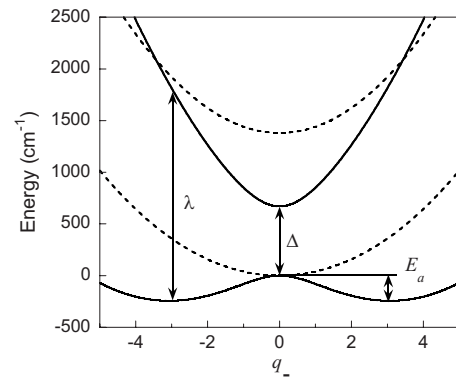

FIG. 4. Adiabatic potential surfaces in the off-diagonal coupling calculated for 15-kD (solid lines) and 270-kD (dashed lines) polymers. Note that we transfer the antisymmetric coordinate Q_- into a dimensionless variable $q_- = \sqrt{2l_-^2/\lambda\hbar\omega_-}Q_-$ to exclude the unknown parameters, e.g., k_- and l_-, in Eq. (4). Charge transport in 15-kD polymer is in the localized regime ($\lambda > \Delta$) and requires activation energy E_a for polaron hopping. Charge transport in 270-kD polymer is in the delocalized regime ($\Delta > \lambda$).
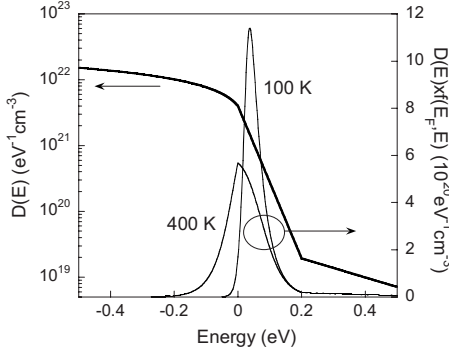
FIG. 5. DOS of polymer for the ME model and carrier density at 400 K and 100 K extracted from fitting the 270-kD P3HT transistor.

IV. CHARGE TRANSPORT MODEL

We now proceed by incorporating the above values for the polaron activation energy into a model of the temperature dependence of the field-effect mobility. We select a simple mobility-edge (ME) model, which provides a better fit of the data than, for example, the variable-range hopping model developed in Ref. 69 as discussed below. The ME model is a semiquantitative model assuming a defined energy (the mobility edge) in the density of states (DOS) which separates mobile states from localized states.[70] The model assumes that only carriers in electronic states above the mobility edge carry current with a constant mobility μ_0, while carriers in localized states below the mobility edge are assumed to make no contribution to the current. For the purpose of the present work one can consider the mobility edge as an effective transport energy to which the carriers need to be thermally activated in order to participate in conduction. Within this framework we follow Bässler *et al.*[22] and incorporate the polaronic effect by assuming that the mobility above the mobility edge is thermally activated with a polaron activation energy taken from the above dynamic vibronic model.

The model is consistent with the experimentally observed temperature dependence of the linear field-effect mobility in the temperature range between room temperature and about 100–150 K which is well described by a thermal activation behavior [see Fig. 2(a)]. We emphasize that in the temperature range discussed here our data, in particular those on TCB samples, are better described by a thermally activated temperature dependence than by the characteristic Efros-Shklovskii hopping temperature dependence for the conductivity $\sigma \propto e^{-\sqrt{T_0/T}}$ claimed in Ref. 71. We explicitly exclude in our description here temperatures below 100–150 K. In this range the mobility shows a weaker temperature dependence that cannot be described by simple activation behavior. In the literature this has been attributed to a finite mobility of carriers hopping in the tail of localized states or hopping in the presence of Coulomb interactions.[71] Note also that all measurements performed here are in the linear regime where electric fields along the channel are small: $E = V_{ds}/L < 2.5$ kV/cm.

Figure 5 shows the DOS used in the calculation. Here the mobility edge is set to $E = 0$ eV. The localized states
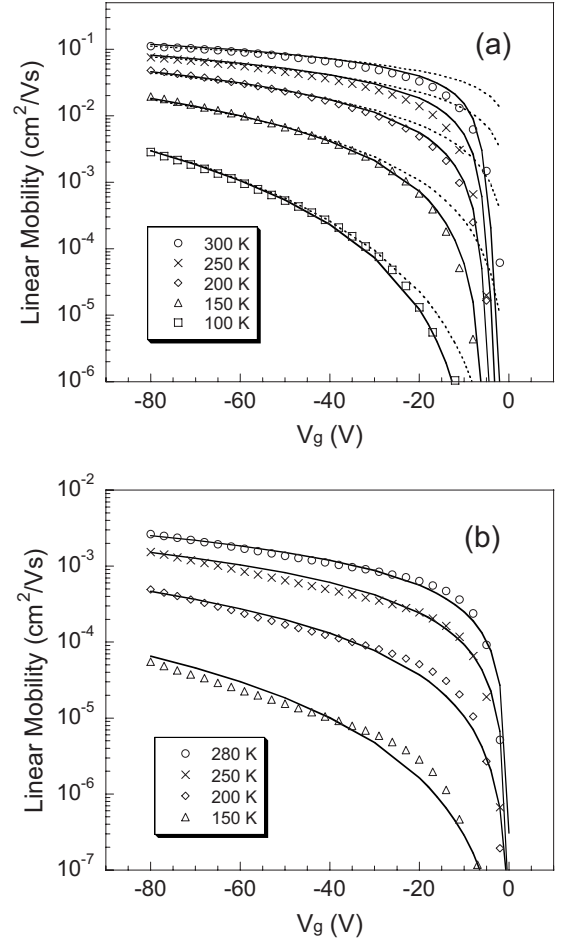

FIG. 6. Experimental data (open symbols) and ME model fit (solid lines) of gate voltage dependent mobility at different temperatures for (a) 270-kD TCB and (b) 15-kD TCB transistors. The dotted lines in (a) show the fitting result if the deep trap states are not included in the ME model.

($E > 0$) of the polymer were represented by two exponential distributions of donor-like states that decay into the band gap, including a shallow trap state for $0 < E < E_{deep}$,

$$D_{tail}(E) = \frac{N_{tail}}{w_{tail}} e^{-E/w_{tail}}, \qquad (7)$$

and a deep trap state for $E > E_{deep}$,

$$D_{deep}(E) = \frac{N_{tail}}{w_{tail}} e^{-E_{deep}/w_{tail}} e^{-(E-E_{deep})/w_{deep}}, \qquad (8)$$

where N_{tail} represents the concentration of tail states and w_{tail} and w_{deep} are the widths of the two exponential trap distributions. The total number of trap states integrated from 0 to infinity can be calculated as $N_{tail}(1 - e^{-E_{deep}/w_{tail}} + w_{deep}/w_{tail} e^{-E_{deep}/w_{tail}})$. The temperature and gate voltage dependences of the mobility are mainly determined by the shallow trap states,[52] but the inclusion of deep states allows a more accurate description of the behavior below the threshold voltage. The DOS of the polymer inside the mobile states

TABLE II. Parameters extracted from fitting the experimental data to the ME model. The parameter values in parentheses are extracted from the model incorporated with polaron activation energy [Eq. (12)].

	E_a [meV]	μ_0 [cm^2/(V s)]	N_{tail} [cm^{-3}]	w_{tail} [meV]	E_{deep} [meV]	w_{deep} [meV]
270 kD TCB[a]	–	0.60	2.3×10^{20}	39	–	–
270 kD TCB	–	0.65	2.4×10^{20}	36.5	200	250
37 kD TCB	–	0.40	2.7×10^{20}	38	200	280
37 kD CH	–	0.13	4.0×10^{20}	46	265	400
	(5)	(0.16)	(3.8×10^{20})	(46)	(260)	(400)
15 kD TCB	–	0.07	6.0×10^{20}	48.5	350	350
	(30)	(0.14)	(3.5×10^{20})	(48)	(320)	(320)

[a]Deep trap states are not included in the ME model. The fitting errors of w_{tail} are about ±1 meV, E_{deep} and w_{deep} about ±20 meV, μ_0 about ±0.05 cm^2/(V s), and N_{tail} about ±0.2×10^{20} cm^{-3} and ±0.5×10^{20} cm^{-3} for high-mobility (270-kD TCB and 37-kD TCB) and low-mobility (37-kD chloroform and 15-kD TCB) devices, respectively.

was described with a simple form for a 3D free hole gas $[D(E) \sim \sqrt{E}]$,[70]

$$D_{mob}(E) = \frac{N_{tail}}{w_{tail}\sqrt{E_v}}\sqrt{E_v - E}, \qquad (9)$$

where E_v is a parameter used to tailor the shape of the DOS inside the band. In our fitting work E_v is fixed at 37 meV as the temperature dependence is rather insensitive to the feature of mobile states.

Since the total amount of gate voltage-induced interface charges is the summation of the charges in the mobile and trap states, the position of the Fermi level $E_F(V_g,T)$ can be obtained by solving

$$N_{tot} = \int_{-\infty}^{\infty} D(E)f(E_F,E)dE \approx \frac{C_i|V_g - V_{on}|}{h}, \qquad (10)$$

where h is the channel dimension normal to the dielectric surface (the model makes the simplifying assumption that all charges are located within an accumulation layer of dimension $h = 1$ nm from the interface) and $f(E_F,E)$ is the Fermi-Dirac distribution of holes. As the temperature decreases, the Fermi level moves towards higher DOS while the Fermi-Dirac distribution becomes narrower and the possibility for charges situated within the mobile states reduces, leading to a decreased mobility. On the other hand, the mobility increases with gate bias due to the Fermi level shifting to a higher DOS. In the polaron-free case, the effective mobility is determined by the ratio of the number of charges located in mobile states above the mobility edge, N_{mob} and N_{tot},

$$\mu(V_g,T) = \mu_0 \frac{N_{mob}(V_g,T)}{N_{tot}}. \qquad (11)$$

In class-II samples in which the polaron activation energy as obtained from the dynamic vibronic model is finite we factorize the effective mobility as the product of a disorder and a polaron term[22]—i.e.,

$$\mu(V_g,T) = \mu_0 \exp(-E_a/k_BT)\frac{N_{mob}(V_g,T)}{N_{tot}}, \qquad (12)$$

where k_B is Boltzmann's constant. Equation (12) assumes that the polaron effect only contributes an additional activation energy to the temperature dependence of the mobility, but does not affect the gate voltage dependence of the mobility which is governed by disorder.

Figures 6(a) and 6(b) show the best fit to the gate-voltage-dependent mobility at different temperatures for the high- and low-MW devices by using Eq. (12) with μ_0, N_{tail}, w_{tail}, E_{deep}, and w_{deep} as free parameters. E_a is not a fitting parameter, but is taken to be the value estimated from the dynamic vibronic model in Sec. III. The fitting parameters compared for polaronic and polaron-free cases are summarized in Table II. First, it can be seen that the model fits well in both the linear and subthreshold regimes. In the linear regime ($V_g \gg V_{ds}$) above threshold the fitting is dominated by the values of N_{tail} and w_{tail}, but less sensitive to the values of E_{deep} and w_{deep}. This is because in this regime the Fermi energy is situated within the shallow trap states far from the deep trap states. However, in the subthreshold regime where V_g approaches V_{ds} (−5 V), the Fermi energy moves towards lower DOS and the fitted curves become sensitive to the values of E_{deep} and w_{deep}. As shown in Fig. 6(a), the model without deep trap states (dotted lines) can also fit the linear regime well with similar values of μ_0, N_{tail}, and w_{tail}, but in the subthreshold regime the mobilities tend to be overestimated by at least an order of magnitude. Our result demonstrates that introducing the deep trap states enables us to account for the more gradual turn-on behavior, as the proportion of the accumulated charges situated within mobile states is significantly reduced compared to the model involving only shallow states. Völkel *et al.* have also shown that the distribution of deep trap states is relevant to the onset voltage and subthreshold slope.[72] Compared with crystalline TCB devices, the larger subthreshold slope of the disorder chloroform devices could be attributed to a broader distribution of deep trap states. The errors of E_{deep} and w_{deep} estimated from the fits are small (±20 meV). Note that for all devices the total
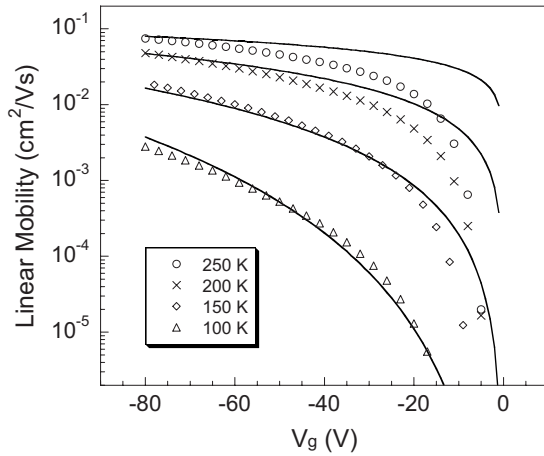
FIG. 7. Vissenberg-Matters hopping model fits (solid lines) to the experimental data (open symbols) of the gate voltage dependent mobility at different temperatures for 270-kD TCB devices.

number of trap states is approximately equal to N_{tail} as $\exp(-E_{deep}/w_{tail}) \ll 1$.

In Table II we also show the effect of including the polaron activation in the ME analysis of the class-II samples. The numbers in brackets for the class-II samples (15 kD TCB and 27 kD chloroform) are extracted when including the finite polaron activation energy found from the dynamic vibronic analysis of the CT transition [Eq. (12)], while the numbers without brackets refer to fits obtained without including the polaron effect [Eq. (11)]. It can be seen that inclusion of polaron activation energy mainly results in a decreased concentration of tail states, N_{tail}, and increased intrinsic mobility μ_0, while there is little change in the bandwidth of tail and deep trap states (w_{tail} and w_{deep}) since the polaron effect does not influence the gate voltage dependence of mobility dominated by these two parameters. As a result of including the polaron activation in class-II samples, the values of N_{tail} and μ_0 become less MW dependent compared to those predicted by the less realistic polaron-free model. Overall, the polaronic ME model shows that the increase of mobility with MW can be mainly attributed to a combined effect of reduced polaron activation energy, higher intrinsic mobilities, and narrower bandwidths of shallow trap states, but there seems to be little reduction in the total number of tail states in the high-MW samples compared to the low-MW ones.

In order to validate our choice of ME transport model we also attempted to fit the temperature-dependent mobility with the Vissenberg-Matters hopping model.[69] However, we found that it is not possible to fit the data well over the whole temperature range (Fig. 7). We chose to fit the gate-voltage-dependent mobility in the low-temperature regime (100–200 K) first to extract values for the overlap parameter α, the conductivity prefactor σ_0, and the width of the exponential DOS, T_0. At low temperatures the hopping mechanism is believed to be dominant for charge transport. An obvious disagreement between the fit and the experimental

data then occurs at elevated temperatures (>200 K), where the mobility predicted by the model tends to be more independent of V_g compared with the experimental data. Moreover, for high-mobility devices the model breaks down around room temperature [Eq. (2) in Ref. 69 diverges]. This finding is consistent with other recent work that has also concluded that the Vissenberg-Matters hopping model is not applicable to high-mobility semicrystalline polymers.[27,52]

V. DISCUSSION AND CONCLUSIONS

We have performed a combined study of temperature-dependent field-effect mobility and low-energy optically induced charge-transfer transitions in order to investigate the effect of polaron formation on activated transport in high-mobility P3HT FETs as a function of MW. We have shown evidence for a transition from a localized polaron regime in low-MW and relatively disordered, lower-mobility samples to a delocalized regime in highly ordered, high-MW samples that exhibit higher mobilities. In the localized regime charges are localized on individual segments of the polymer chain and the polaronic reorganization energy makes a significant contribution to the thermal activation energy of the field-effect mobility. In the delocalized regime charges are not confined to individual segments of the polymer chain and are assumed to be delocalized over a number of neighboring chain segments. In this regime the field-effect mobility is entirely limited by residual disorder and polaronic relaxation makes no significant contribution to the thermal activation of the mobility.

The values for the polaron activation energy of P3HT in the localized regime are considered reasonable if compared with values reported in the literature. For isolated pentacene molecules the total reorganization energy has been estimated to be about 100 meV on the basis of density functional theory calculations.[73] This renders a polaron activation energy of 25 meV in a nonadiabatic transition and even lower if strong electronic coupling is involved in the ET process. In comparison, our analysis using Piepho's model predicts a polaron activation energy in the range of 5–30 meV for P3HT samples that are in the localized class-II regime which is of a similar order as that predicted for pentacene.

We emphasize that Piepho's model used in this paper was developed for a dimer system and therefore has certain limitations when applied to a complex polymer system. First, the disorder is not taken into account in Piepho's model. One may expect that energetic disorder between two neighboring molecules will contribute to the modulation of the reorganization energy and electronic coupling. In the analysis of the CT transition presented here disorder was included only by including some inhomogeneous broadening of each vibronic line to smoothen the simulated spectra. Indeed, the linewidth Γ obtained in our calculations is generally larger by a factor of 2–3 than those obtained in dimeric systems, and this also accounts for the nonzero calculated intensity at the origin of energy (see Fig. 3). To improve on this model disorder will have to be taken into account at the level of the vibronic Hamiltonian. Second, since Piepho's model only considers the electron transfer between two molecules via electron-

phonon coupling, it may strictly only be applicable in the class-I and -II regimes, but may not be satisfactory for the high-mobility polymer samples in the class-III regime where polarons are delocalized over more than two molecules. This may partly explain why we extract a very large decrease of reorganization energy λ from low- to high-MW polymers. The values of λ in the localized regime are believed to be sensible since this regime is consistent with the assumption of Piepho's model, but they are likely to be inaccurate in the strongly delocalized regime. However, we emphasize that this limitation of the model does not affect our key conclusion that in P3HT polymers of low and high MW a crossover from a class-I/II to a class-III transport regime occurs.

Our theoretical calculations show accuracy towards smaller reorganization energy λ and larger electronic coupling parameters Δ in devices with higher mobilities. To investigate the sensitivity of the results to the values of the input parameters of the vibronic model we have varied the parameter values for $\hbar\omega_-$, $\hbar\omega_+$, and Γ over a reasonably wide range. We have found that independent of the parameter values the general trend between different devices remains the same and also the estimated values for polaron activation energy and transfer integral are not changed significantly. In general, by varying $\hbar\omega_-$ within a range of 50–500 cm^{-1} and $\hbar\omega_+$ within 500–1450 cm^{-1} the polaron activation energy extracted from the fitting parameters varies approximately between 30 and 40 meV in 15-kD TCB devices and 5–10 meV in 37-kD chloroform devices. For high-mobility devices the fitting result is less sensitive to the choice of the parameter values. Therefore, we believe that Piepho's model is able to capture the essential physical insight into the electron-transfer process in these high-mobility polymers. Further extension of the vibronic model to include disorder and larger molecular aggregates is expected to provide a more accurate, quantitative estimation of polaron activation energy and transfer integrals.

The transition from the localized to the delocalized regime is believed to be driven by longer intrachain conjugation lengths and more pronounced interchain interactions in the high-MW samples. It has previously been shown that strong interchain interactions are responsible for charge carriers in high-mobility P3HT acquiring a two-dimensional interchain character.[41,59,74,75] Similarly, in oligomeric systems it has also been shown that the polaron relaxation energy decreases as conjugation length increases.[75] In our previous work[30] we have investigated polymer chain microstructure in nanoribbon microcrystals of P3HT as a function of MW. Based on structural characterization as well as analysis of optical absorption and emission spectra evidence was obtained for the short chains of low-MW polymers folding into conjugated lamellae with a higher population of chain end defects, resulting in a shorter conjugation length and locally perturbed interchain packing. This is believed to be responsible for the more localized intrachain nature of the polarons and the relatively high polaron activation energy. As MW increases, folding of longer chains produces fewer defects in the conjugated lamellae. Such an improvement in crystalline quality leads to a longer conjugation length and less

perturbed interchain packing and, as a result, a higher degree of polaron delocalization and hence lower polaron activation energy. The present results are supported by theoretical calculations predicting that the polaronic effect may entirely disappear due to strong interchain interactions unless stabilized by conjugation defects or chain breaks.[76]

The inclusion of the polaron activation energy in an analysis of the temperature and gate voltage dependences of the field-effect mobility enables a more realistic assessment of the disordered DOS distribution of the polymer as a function of MW than could be achieved by models that ignore the polaron activation. When taking the polaron activation energy into account in the ME model we have shown that the total concentration of trap states ($\sim N_{tail}$) is almost independent of MW; i.e., it varies by less than a factor of 2 within the range of MWs investigated ($N_{tail} \approx 2$–3×10^{20}/cm^3). To obtain an idea about the nature of this tail states we can estimate the number of tail states per P3HT nanoribbon. The width of a P3HT nanoribbon is 15 nm for 15.4 kD and 20 nm for 270 kD (see Ref. [30]). We assume the accumulation layer to be 1 nm thick and neglect the interfacial area taken up by grain boundaries. The spacing between two π-stacked lamellae is 3.8 Å. This yields an estimate of about two traps in an interfacial area within the accumulation layer that is defined by the typical width of a nanoribbon and the spacing between π-stacked polymer chains—i.e., the interfacial area that is occupied by one chain inside a nanoribbon. This number is nearly independent of MW. This estimate suggests that structural or chemical defects other than chain ends, such as defects associated with chain folding on the surface of the nanocrystals or conjugation defects inside the nanoribbon, will also contribute to the tail state distribution. The polaronic ME model analysis implies that the distribution of tail states depends sensitively on MW, while the number of tail states does not vary strongly with MW. Higher-MW polymers have a narrower band tail width than low-MW polymers. This might imply that although the density of structural defects in the nanocrystals does not depend strongly on the length of the polymer chain, the energetic broadening of the DOS associated with these defects is enhanced by the presence of chain ends and other defects present in the nanocrystals of the low-MW polymers.

In conclusion, we have presented a detailed study of the contribution polaron activation makes to the observed temperature dependence of P3HT FETs. Through an analysis of the charge-induced absorption spectra we have extracted quantitative values for the reorganization energy λ and the electronic coupling integral Δ for charges in the accumulation layer of P3HT FETs of different MW. The analysis reveals that charge transport with mobilities of the order of 10^{-3} cm^2/(V s) is in a localized regime in which polaron activation cannot be neglected, while in films with mobilities exceeding 10^{-2} cm^2/(V s) charge carriers are delocalized over several neighboring chains and polaron relaxation is not observable in the electrical device characteristics. Our study indicates that the polaron effect decreases much faster than the disorder effect as MW increases and the disorder remains the mobility-limiting factor in high-MW, high-mobility devices. Therefore, in order to realize higher mo-

bilities, it is necessary to improve crystalline quality and reduce disorder by using polymers that are less prone to structural defects[77] or by employing growth techniques that allow better control over the defects incorporated into the polymer nanocrystals.[78]

*Corresponding author. hs220@phy.cam.ac.uk

[1] H. Scher and E. W. Montroll, Phys. Rev. B **12**, 2455 (1975).

[2] H. Bässler, Phys. Status Solidi B **175**, 15 (1993).

[3] N. Apsley and H. P. Hughes, Philos. Mag. **30**, 963 (1974).

[4] G. P. Triberis, J. Phys. C **20**, 3707 (1987).

[5] T. Holstein, Ann. Phys. (N.Y.) **8**, 325 (1959).

[6] T. Holstein, Ann. Phys. (N.Y.) **8**, 343 (1959).

[7] D. Emin, Phys. Rev. Lett. **25**, 1751 (1970).

[8] D. Emin, Phys. Rev. B **4**, 3639 (1971).

[9] D. Emin, Adv. Phys. **25**, 305 (1975).

[10] N. F. Mott, *Electronic and Structural Properties of Amorphous Semiconductors*, edited by P. G. LeComber and J. Mort (Academic, London, 1973).

[11] A. Miller and E. Abrahams, Phys. Rev. **120**, 745 (1960).

[12] L. B. Schein, A. Rosenberg, and S. L. Rice, J. Appl. Phys. **60**, 4287 (1986).

[13] L. B. Schein, D. Glatz, and J. C. Scott, Phys. Rev. Lett. **65**, 472 (1990).

[14] A. Peled and L. B. Schein, Chem. Phys. Lett. **153**, 422 (1988).

[15] P. M. Borsenberger, L. Pautmeier, and H. Bässler, J. Chem. Phys. **94**, 5447 (1991).

[16] P. M. Borsenberger, J. Appl. Phys. **68**, 5682 (1990).

[17] M. A. Abkowitz and M. Stolka, Philos. Mag. Lett. **58**, 239 (1988).

[18] S. V. Novikov, D. H. Dunlap, V. M. Kenkre, P. E. Parris, and A. V. Vannikov, Phys. Rev. Lett. **81**, 4472 (1998).

[19] W. F. Pasveer, J. Cottaar, C. Tanase, R. Coehoorn, P. A. Bobbert, P. W. M. Blom, D. M. de Leeuw, and M. A. J. Michels, Phys. Rev. Lett. **94**, 206601 (2005).

[20] E. H. Magin and P. M. Borsenberger, J. Appl. Phys. **73**, 787 (1993).

[21] M. Van der Auweraer, F. C. De Schryver, P. M. Borsenberger, and H. Bässler, Adv. Mater. (Weinheim, Ger.) **6**, 199 (1994).

[22] H. Bässler, P. M. Borsenberger, and R. J. Perry, J. Polym. Sci., Part B: Polym. Phys. **32**, 1677 (1994).

[23] V. M. Kenkre and D. H. Dunlap, Philos. Mag. B **65**, 831 (1992).

[24] D. H. Dunlap and V. M. Kenkre, Chem. Phys. **178**, 67 (1993).

[25] P. E. Parris, V. M. Kenkre, and D. H. Dunlap, Phys. Rev. Lett. **87**, 126601 (2001).

[26] I. I. Fishchuk, A. Kadashchuk, H. Bässler, and S. Nespurek, Phys. Rev. B **67**, 224303 (2003).

[27] H. Sirringhaus, Adv. Mater. (Weinheim, Ger.) **17**, 2411 (2005).

[28] Y. Y. Deng and H. Sirringhaus, Phys. Rev. B **72**, 045207 (2005).

[29] J. Cornil, D. Beljonne, J.-P. Calbert, and J.-L. Brédas, Adv. Mater. (Weinheim, Ger.) **13**, 1053 (2002).

[30] J.-F. Chang, J. Clark, N. Zhao, H. Sirringhaus, D. W. Breiby, J. W. Andreasen, M. M. Nielsen, M. Giles, M. Heeney, and I. McCulloch, Phys. Rev. B **74**, 115318 (2006).

[31] C. Creutz and H. Taube, J. Am. Chem. Soc. **91**, 3988 (1969).

[32] C. Creutz, Prog. Inorg. Chem. **30**, 1 (1983).

[33] R. S. Mulliken, J. Am. Chem. Soc. **74**, 811 (1952).

[34] G. Allen and N. S. Hush, Prog. Inorg. Chem. **8**, 357 (1967).

[35] R. A. Marcus, J. Chem. Phys. **24**, 966 (1956).

[36] R. A. Marcus and N. Sutin, Comments Inorg. Chem. **5**, 119 (1986).

[37] R. A. Marcus and N. Sutin, Biochim. Biophys. Acta **811**, 265 (1985).

[38] M. Robin and P. Day, Adv. Inorg. Chem. Radiochem. **10**, 247 (1967).

[39] N. S. Hush, Prog. Inorg. Chem. **8**, 391 (1967).

[40] N. S. Hush, Coord. Chem. Rev. **64**, 135 (1985).

[41] H. Sirringhaus, P. J. Brown, R. H. Friend, M. M. Nielsen, K. Bechgaard, B. M. W. Langeveld-Voss, A. J. H. Spiering, R. A. J. Janssen, E. W. Meijer, P. Herwig, and D. M. De Leeuw, Nature (London) **401**, 685 (1999).

[42] P. J. Brown, H. Sirringhaus, M. Harrison, M. Shkunov, and R. H. Friend, Phys. Rev. B **63**, 125204 (2001).

[43] O. J. Korovyanko, R. Österbacka, X. M. Jiang, Z. V. Vardeny, and R. A. J. Janssen, Phys. Rev. B **64**, 235122 (2001).

[44] R. Österbacka, C. P. An, X. M. Jiang, and Z. V. Vardeny, Science **287**, 842 (2000).

[45] D. Beljonne, J. Cornil, H. Sirringhaus, P. J. Brown, M. Shkunov, R. H. Friend, and J.-L. Brédas, Adv. Funct. Mater. **11**, 229 (2001).

[46] S. B. Piepho, E. R. Krausz, and P. N. Schatz, J. Am. Chem. Soc. **100**, 2996 (1978).

[47] S. B. Piepho, J. Am. Chem. Soc. **110**, 6319 (1988).

[48] S. B. Piepho, J. Am. Chem. Soc. **112**, 4197 (1990).

[49] V. Coropceanu, M. Malagoli, J. M. Andre, and J. L. Brédas, J. Am. Chem. Soc. **124**, 10519 (2002).

[50] G. Koller, B. Falk, C. Weller, M. Giles, and I. McCulloch, Process of preparing regioregular poly-(3-substituted) thiophenes., PCT Int. Appl., WO2005014691 (2005).

[51] B. H. Hamadani and D. Natelson, Appl. Phys. Lett. **84**, 443 (2004).

[52] A. Salleo, T. W. Chen, A. R. Völkel, Y. Wu, P. Liu, B. S. Ong, and R. A. Street, Phys. Rev. B **70**, 115311 (2004).

[53] E. J. Meijer, C. Tanase, P. W. M. Blom, E. van Veenendaal, B.-H. Huisman, D. M. deLeeuw, and T. M. Klapwijk, Appl. Phys. Lett. **80**, 3838 (2002).

[54] R. A. Street, J. E. Northrup, and A. Salleo, Phys. Rev. B **71**, 165202 (2005).

[55] A. R. Brown, C. P. Jarrett, D. M. deLeeuw, and M. Matters, Synth. Met. **88**, 37 (1997).

[56] J.-F. Chang, B. Q. Sun, D. W. Breiby, M. M. Nielsen, T. I. Sölling, M. Giles, I. McCulloch, and H. Sirringhaus, Chem. Mater. **16**, 4772 (2004).

[57] A. Zen, J. Pflaum, S. Hirschmann, W. Zhuang, F. Jaiser, U. Asawapirom, J. P. Rabe, U. Scherf, and D. Neher, Adv. Funct. Mater. **14**, 757 (2004).

[58] B. Hartenstein, H. Bässler, S. Heun, P. Borsenberger, M. Van der Auweraer, and F. C. De Schryver, Chem. Phys. **191**, 321 (1995).

[59] X. M. Jiang, R. Österbacka, O. Korovyanko, C. P. An, B. Horovitz, R. A. J. Janssen, and Z. V. Vardeny, Adv. Funct. Mater. **12**, 587 (2002).

[60] R. Österbacka, X. M. Jiang, C. P. An, B. Horovitz, and Z. V. Vardeny, Phys. Rev. Lett. **88**, 226401 (2002).

[61] K. Hannewald, V. M. Stojanovic, J. M. T. Schellekens, P. A. Bobbert, G. Kresse, and J. Hafner, Phys. Rev. B **69**, 075211 (2004).

[62] V. Coropceanu, J. Cornil, D. A. da Silva Filho, Y. Olivier, R. Silbey, and J.-L. Brédas, Chem. Rev. (Washington, D.C.) **107**, 926 (2007).

[63] V. Coropceanu, M. Malagoli, J. M. Andre, and J. L. Brédas, J. Chem. Phys. **115**, 10409 (2001).

[64] R. A. Marcus, Discuss. Faraday Soc. **29**, 21 (1960).

[65] N. S. Hush, Electrochim. Acta **13**, 1005 (1968).

[66] C. Lambert and G. Nöll, J. Am. Chem. Soc. **121**, 8434 (1999).

[67] A. Troisi and G. Orlandi, J. Phys. Chem. B **110**, 4065 (2006).

[68] G. Louarn, M. Trznadel, J. P. Buisson, J. Laska, A. Pron, M. Lapkowski, and S. Lefrant, J. Phys. Chem. **100**, 12532 (1996).

[69] M. C. J. M. Vissenberg and M. Matters, Phys. Rev. B **57**, 12964 (1998).

[70] R. A. Street, *Hydrogenated Amorphous Silicon* (Cambridge University Press, Cambridge, England, 1991).

[71] A. S. Dhoot, G. M. Wang, D. Moses, and A. J. Heeger, Phys. Rev. Lett. **96**, 246403 (2006).

[72] A. R. Völkel, R. A. Street, and D. Knipp, Phys. Rev. B **66**, 195336 (2002).

[73] V. Coropceanu, M. Malagoli, D. A. da Silva Filho, N. E. Gruhn, T. G. Bill, and J. L. Brédas, Phys. Rev. Lett. **89**, 275503 (2002).

[74] P. J. Brown, D. S. Thomas, A. Köhler, J. S. Wilson, J.-S. Kim, C. M. Ramsdale, H. Sirringhaus, and R. H. Friend, Phys. Rev. B **67**, 064203 (2003).

[75] M. Wohlgenannt, X. M. Jiang, and Z. V. Vardeny, Phys. Rev. B **69**, 241204(R) (2004).

[76] H. A. Mizes and E. M. Conwell, Phys. Rev. Lett. **70**, 1505 (1993).

[77] I. McCulloch, M. Heeney, C. Bailey, K. Genevivius, I. Macdonald, M. Shkunov, D. Sparrowe, S. Tierney, R. Wagner, W. Zhang, M. L. Chabinyc, R. J. Kline, M. D. McGehee, and M. F. Toney, Nat. Mater. **5**, 328 (2006).

[78] D. H. Kim, J. T. Han, Y. D. Park, Y. Jang, J. H. Cho, M. Hwang, and K. Cho, Adv. Mater. (Weinheim, Ger.) **18**, 719 (2006).